Measurement of the two-photon absorption cross-section of liquid argon with a time projection chamber

Measurement of the two-photon absorption cross-section of liquid argon with a time projection chamber

I Badhrees[1], **A Ereditato**[1], **I Kreslo**[1], **M Messina**[1], **U Moser**[1], **B Rossi**[1,3], **M S Weber**[1], **M Zeller**[1], **C Altucci**[2], **S Amoruso**[2], **R Bruzzese**[2] and **R Velotta**[2]

[1] Albert Einstein Centre for Fundamental Physics Laboratory for High Energy Physics (LHEP) University of Bern, Switzerland
[2] Dipartimento di Scienze Fisiche Università di Napoli 'Federico II' Napoli, Italy
E-mail: biagio.rossi@lhep.unibe.ch

Abstract. This paper reports on laser-induced multiphoton ionization at 266 nm of liquid argon in a time projection chamber (LAr TPC) detector. The electron signal produced by the laser beam is a formidable tool for the calibration and monitoring of next-generation large-mass LAr TPCs. The detector that we designed and tested allowed us to measure the two-photon absorption cross-section of LAr with unprecedented accuracy and precision: $\sigma_{ex} = (1.24 \pm 0.10_{stat} \pm 0.30_{syst}) \times 10^{-56} \, \mathrm{cm^4 \, s^{-1}}$.

[3] Author to whom any correspondence should be addressed.

IOP Institute of Physics ⏀ DEUTSCHE PHYSIKALISCHE GESELLSCHAFT

Contents

1. Introduction

Liquid argon time projection chamber (LAr TPC) detector technology allows for uniform and high-resolution imaging of massive detector volumes. The operating principle of the LAr TPC is based on the undistorted transport of tracks of ionization electrons in highly purified LAr by a uniform electric field over distances up to a few metres. Imaging is provided by wire planes or other readout devices placed at the end of the drift path. The drifting electrons are collected by the outermost wire plane, which gives positional and calorimetric information. Additional planes with different orientation can be positioned in front of the collection plane to record the signal induced by the passage of the drifting electrons. This provides different projective views of the same event, thus allowing space point reconstruction. The coordinate parallel to the drift field is given by measurements of the drift time given by the time interval between the passage of the ionizing particle in the active volume (t_0) and the arrival of the drifting electrons on the wire planes. The t_0 can come from the detection of the scintillation light of LAr by means of photomultipliers (PMTs), or from an external source. The momentum of an incoming particle is inferred by the measurement of its multiple scattering [1], while the detection of local energy deposition provides particle identification. For more information, the reader is referred to [2] and references therein.

The purity of LAr is a key ingredient to achieve imaging over long drift distances. A purity corresponding to less than 0.1 ppb of electronegative elements such as oxygen has to be achieved in order to allow for electron lifetimes of milliseconds, and hence drift distances of metres, as envisioned for large-scale applications of this technique [3]–[7]. This can be obtained by means of commercial purification cartridges and by argon recirculation.

The purity of LAr has to be monitored continuously while the TPC is running, thus calling for practical and efficient purity monitoring techniques. To this end, laser-based methods are very interesting as they provide a reliable route to tackle the problem. In addition, a laser beam is an ideal tool for performing the energy calibration of the detector, for measuring the drift velocity, the space and time resolution of the detector, the capability of double track separation and the diffusion of drifting electrons, and also for verifying the homogeneity of the drift field.
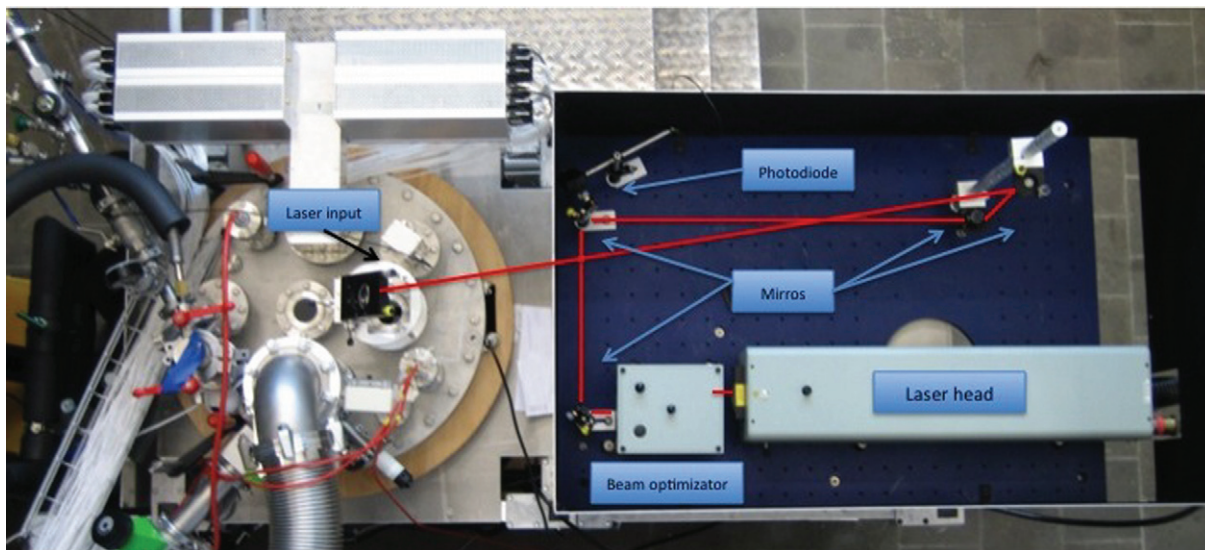
Figure 1. Photograph of the experimental setup (top view) including the laser beam. Red lines show the beam path before being steered into the detector.

In this paper, we report the analysis of the UV laser multiphoton ionization of LAr with the fourth harmonic of a Nd-YAG laser. We used a LAr TPC both as a target medium and as a detector of the electrons produced by the laser radiation.

The interaction of laser light with liquid matter is comparatively less studied with respect to gas and solid phases. Nevertheless, some important features are well understood [8]. Laser ionization can occur as a multiphoton process through the simultaneous absorption of two or more photons via virtual states in a medium. This process requires high photon flux; namely, pulsed lasers. In a multiphoton process, bound electrons absorb several laser photons simultaneously, thus exciting the atom to high-energy levels or even to ionization.

The sole measurements of multiphoton ionization in LAr reported so far were carried out by Sun *et al* in 1996 [9]. An accurate measurement of the two-photon absorption cross-section of LAr (σ_{ex}), which is the atomic intermediate step to ionization, is fundamental for the reliable calibration of LAr TPCs. In [9], an estimate of the range of σ_{ex} is given. Improvements in front-end electronics and data acquisition (DAQ) systems over the last 15 years, and an increase in knowledge of LAr technology, allow us today to measure the two-photon absorption cross-section of LAr with unprecedented accuracy and precision.

The measurements described in this paper were performed with the LAr TPC described in [2]. This was part of an R&D project we carried out in Bern in view of the realization of LAr TPC detectors of increasing size. Results have also been published on the study of a TPC built and operated employing a mixture of LAr and nitrogen [10].

2. Experimental setup

The detector (figure 1) used for the measurements consists of a TPC (figure 2) housed in a cylinder filled with purified LAr, in thermal contact with a bath of LAr (figure 3). The TPC is complemented by an electronic readout and DAQ system, a LAr recirculation and purification
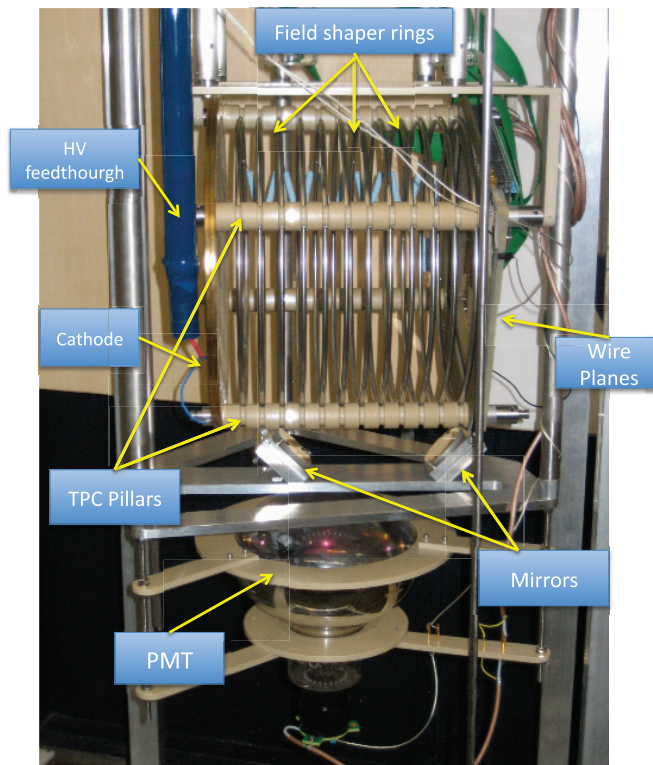
Figure 2. Photograph of the inner part of the detector. The TPC, the PMT, the high voltage (HV) feedthrough and two mirrors installed on a stainless-steel support are visible. The drift direction is horizontal.

system, a PMT, a series of ancillary equipment for monitoring and control, and a UV laser with related optics to allow the study of multiphoton ionization of LAr.

The TPC detector is contained in a stainless-steel cylindrical tube. The latter measures 50 cm in diameter and 110 cm in height, for an inner volume of about 200 litres. The tube is placed in thermal contact with a bath of LAr and is closed by a stainless-steel flange. A series of additional smaller flanges are positioned on the top flange. They include feedthroughs needed to evacuate the inner volume of the vessel, to fill it with LAr, to read out the detector signals, to supply the high voltage, to house the pressure monitors, level meter and safety valves, and to provide the transport of UV laser beams to the inner part of the TPC. The various components are described in detail in [2].

Figure 4 shows the arrangement and the path of the laser beam used for the measurements. The laser beam passes through a system of prisms to be *cleaned* from the residuals of the first and second harmonic components. After a deflection on a 266 nm coated mirror, it is then fed into a variable, motorized attenuator. After the attenuator, two parallel beams of variable intensity are present. One is dumped, while the other is used for the measurements. The use of the attenuator is important, as it allows one to vary the energy of the laser beam without changing the laser generation parameters. Consequently, the laser shows better performance stability. Both energy and pulse length measurements are performed before the beam is finally steered into the chamber.
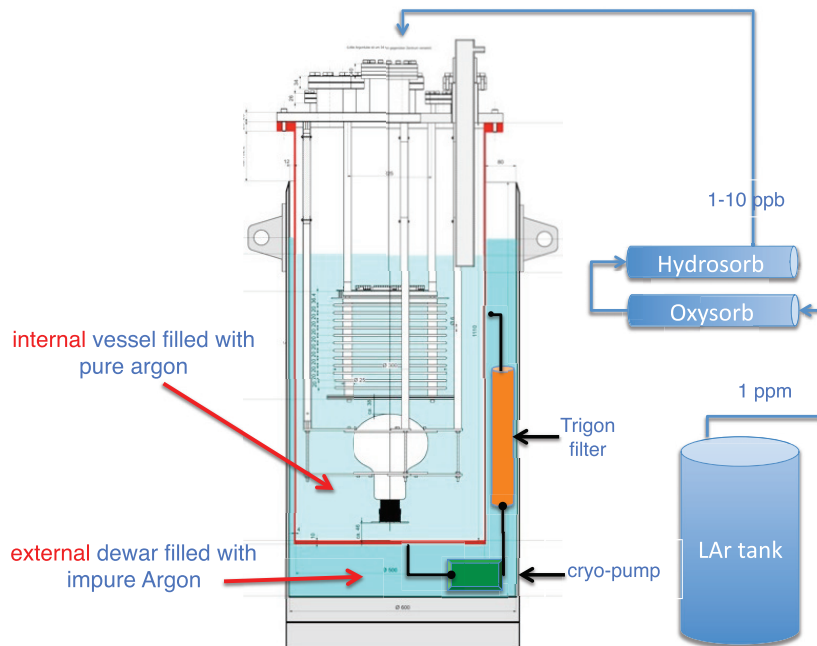
Figure 3. Schematic drawing of the detector setup. The TPC, mounted with the drift coordinate vertically. The PMT and the relative supports are housed in a cylindrical tube filled with pure argon. The external vessel that contains unpurified argon hosts the liquid purification/recirculation system.

In theoretical calculations (section 4.2), we assume for simplicity that the transverse distribution of the laser intensity has a square shape. In the experiment, the laser beam passes after the attenuator through a diaphragm of 4 mm diameter, selecting the more uniform, central part of the beam. In this way one obtains a definite beam cross-section, also preventing any effect of the laser beam tails (halo) on the ionization process. In fact, the contribution to the ionization of photons in the halo is negligible due to the nonlinear character of the process.

After the diaphragm, light is fed into the TPC inner volume by passing through a system of mirrors (figure 1) and a custom-made optical feedthrough [2].

As described in figure 4, the beam passes twice in the active volume, thus producing two parallel tracks at different drift times. After the second passage, the beam is steered out of the dewar by means of another optical feedthrough. The extraction of the laser beam from the TPC allows for the monitoring of its intensity, after ionization of LAr has occurred. The attenuation of the intensity due to the optical feedthroughs and mirrors has been separately measured without LAr in the setup.

The measurement of the pulse width is performed by means of a fast photodiode[4], calibrated in energy with an energy meter[5] and readout by a CAEN V1729 ADC. The board, a switched-capacitor digitizer, performs the coding of four analog channels of bandwidth up to 300 MHz over 12 bits at a sampling frequency of up to 2 GS s^{-1} and over a depth of 2520 usable points. It is suited for the acquisition of fast analog signals.

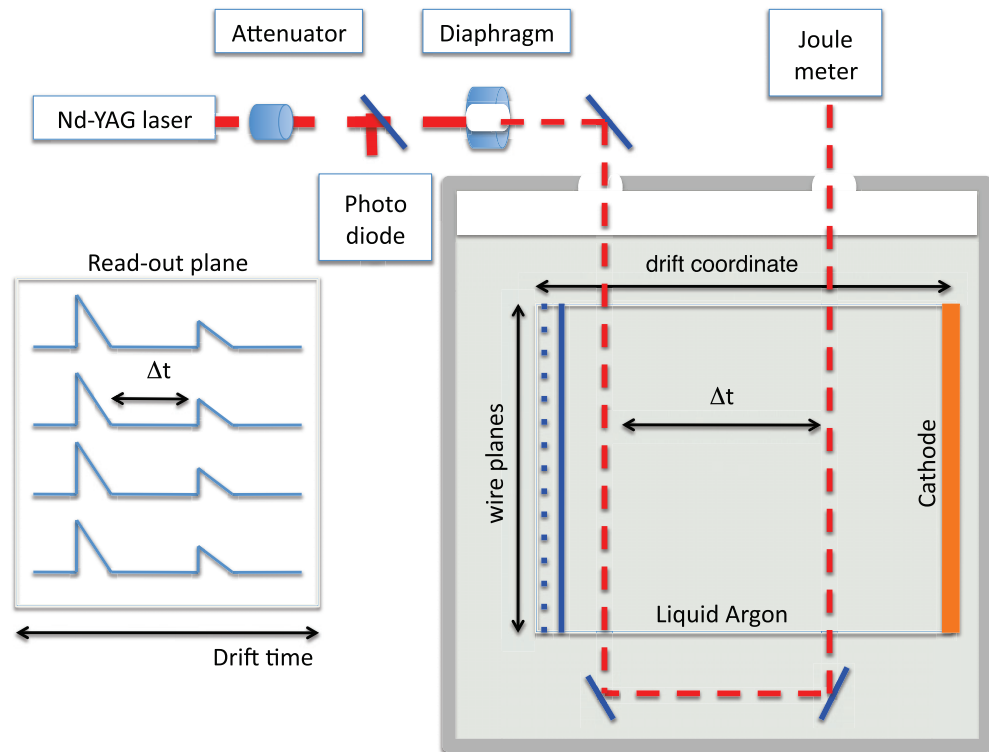[4] Thorlabs DET 10 A.
[5] GEANTEC—SOLO 2.

Figure 4. Schematic view of the laser beam path and the readout response.

3. Detector operation and data taking

Before filling with LAr, the detector vessel is evacuated to a residual pressure of 10^{-5} mbar. The detector is then filled with ultrapure LAr flowing through the purification cartridges in liquid phase, analogous to the purification unit inserted in the recirculation system. The purity of LAr before passing through the OXYSORB and HYDROSORB [11] cartridges has a nominal concentration of water and oxygen of the order of a ppm. The procedure is described in detail in [2].

Several measurements were performed with the TPC installed with electrons drifting along the horizontal direction. The detection of the first UV laser-induced ionization tracks has been published in [2].

The monitoring of the laser photon flux was performed pulse to pulse. In figure 5, the display of a typical UV laser-induced event is shown. Two parallel tracks along all the wires at different drift times are well visible. The beam first generates the same signal over all the wires of the TPC collection plane at the same time (drift coordinate), and then, after the reflection on two mirrors, the beam passes through the active volume, again inducing another track parallel to the first one. In figure 6, typical waveform peaks induced by a single UV laser pulse on a collection wire are shown. Two peaks at different drift times are clearly visible. In this configuration, for each laser pulse we have 64 independent measurements of the electron yield produced by the first and second tracks. Combining the information from the two wire planes, a three-dimensional reconstruction of the track is performed. From the collection plane, calorimetric information about the electron yield by the laser beam is retrieved.
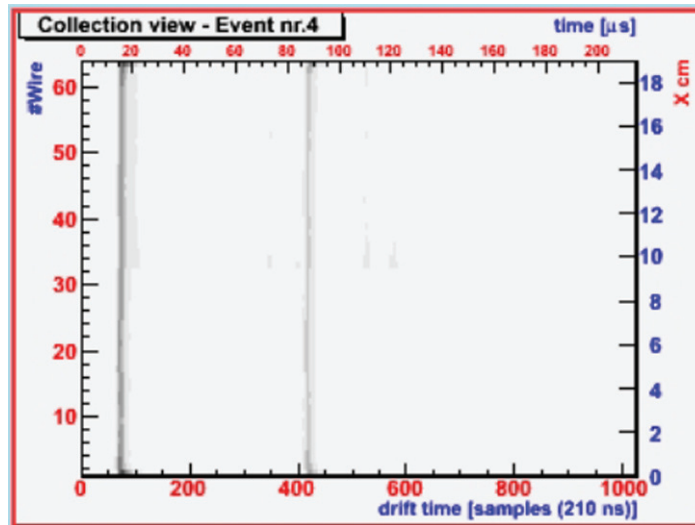
Figure 5. Display of a UV laser ionization event. Two parallel tracks inducing a signal on 64 wires at different drift times (at samples 75 and 420) are visible. Wire number 64 corresponds to the point at which the beam first enters in the TPC.
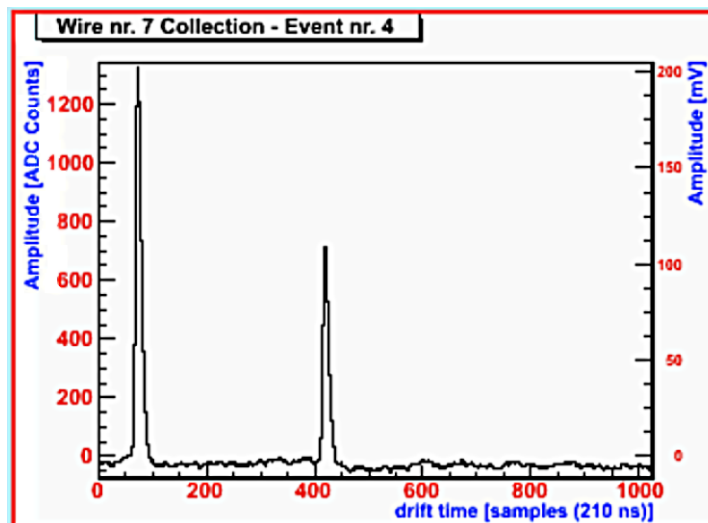
Figure 6. Typical signals induced on a wire of the TPC collection plane by the two UV laser-induced tracks. Two peaks at different drift times are clearly visible. The area under each peak provides the electron yield.

The distance between the first (second) track and the wire planes is 28 mm (183 mm). From the distance between the laser tracks (155 mm) and the measurement of the difference between the drift times of the two peaks (wire by wire), one can determine the electron drift speed. Finally, from the ratio of the area under the two peaks, we can measure the electron attachment to electronegative impurities and therefore the actual purity of LAr.

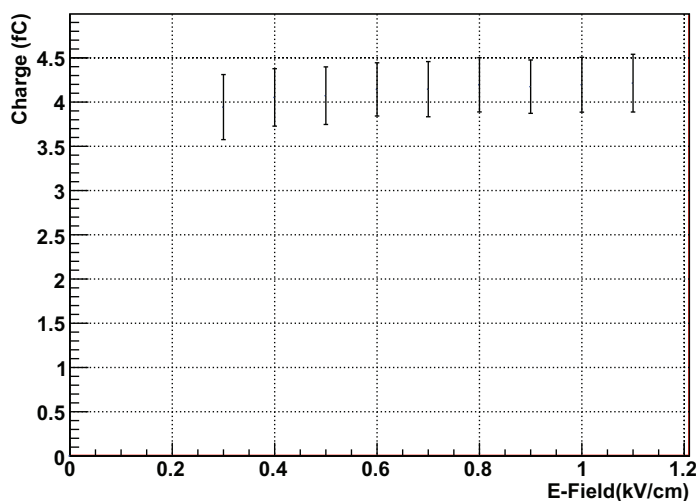**Figure 7.** Plot of the charge produced by a UV laser beam as a function of drift electric field. This plot shows that charge recombination is insignificant for UV laser beam-induced events with respect to events with minimum ionizing particles. At an operational drift field value of $1\,\mathrm{kV\,cm^{-1}}$, charge recombination can be neglected.

The electron attachment to the electronegative impurities present in LAr during drift and charge recombination diminishes the charge collected by the wire planes, affecting the reconstruction of the number of electrons produced by laser beams. During the data taking, both the LAr purity and charge recombination were measured, and therefore the correction factors were applied to the data presented in section 5.

The concentration of electronegative impurities was at the level of 1 ppb of O_2 eq., leading to an attenuation length of about $\lambda = 650\,\mathrm{mm}$ with a drift field of $1\,\mathrm{kV\,cm^{-1}}$ for the drifting electrons, a factor about 20 times larger than the distance between the first track and the wire planes.

The effect of charge recombination was retrieved by the data of figure 7, which shows the charge collected by a single wire, produced by UV laser beams, as a function of drift electric field. For this set of data, the laser repetition rate was $10\,\mathrm{Hz}$ and the energy per pulse was about $1.0\,\mathrm{mJ}$. Nine different runs of 1000 events for each drift field value were recorded. Data were taken during 10 min, in order to have the same purity conditions for each run. Each entry of the plot of figure 7 is the mean value (and the RMS) of the charge distribution for each run. Only information provided by the laser track closest to the wire planes is considered for this analysis. The laser peak-to-peak energy instability (about 5%), the energy resolution of the TPC and the uncertainties introduced by the reconstruction algorithm contribute to the ordinate's error bars.

For drift fields above $E \geqslant 0.5\,\mathrm{kV\,cm^{-1}}$, the data points lie on a flat line, indicating that charge recombination for this region is negligible. For drift fields below $E < 0.5\,\mathrm{kV\,cm^{-1}}$, an indication of a decrease in collected charge appears, but no statistically significant statements can be made. This shows that charge recombination is insignificant for UV laser beam-induced events compared to events with ionizing particles, for which the recombination at $0.5\,\mathrm{kV\,cm^{-1}}$ is about 25%.

This difference is likely due to the fact that the charge produced by laser beams is distributed over a much larger volume, i.e. the transverse laser beam spot (diameter $\sim 3\,\text{mm}$) is much larger than the point-like spot of a minimum ionizing particle (m.i.p.) track. Although the total number of electrons produced by the laser can be large (up to several hundreds of m.i.p. equivalent), the resulting space charge density for laser ionization is thus much smaller than for m.i.p., and charge recombination effects may indeed be insignificant.

Since the operational field used for the cross-section measurement reported in this paper was $1\,\text{kV cm}^{-1}$, we neglect the recombination effect in our data and in the calculation presented in section 4.2.

The fact that we found negligible charge recombination for laser ionization is interesting for understanding the recombination mechanism and is currently a matter of further investigation. A detailed study of the possible dependence of charge recombination on laser beam energy will be the subject of our forthcoming studies.

4. Multiphoton absorption of liquid argon (LAr)

An atom with ionization energy E_i can be ionized by irradiation with photons having energy $E = h\nu$ much lower than E_i if the photon flux is intense enough to promote multiphoton absorption.

One of the features of multiphoton absorption is that it can occur via laser-induced virtual states, which are not eigenstates of the atom. Thus, it does not require any intermediate atomic state. These laser-induced virtual states are characterized by a lifetime τ^{virtual} of the order of one optical cycle. For the laser used in this experiment, we have

$$\tau_{266\,\text{nm}}^{\text{virtual}} \approx \frac{\lambda}{2\pi c} \approx 1.4 \times 10^{-16}\,\text{s}, \tag{1}$$

while the lifetime of an intermediate (excited) *real* state is of the order of $\tau \sim 10^{-8}\,\text{s}$ [12]. When an atomic state is located not too far from a laser-induced virtual state (quasi-resonant ionization), the multiphoton absorption process is strongly enhanced, thus requiring a laser intensity much lower than in the non-resonant case [12].

4.1. Energy levels in LAr

The interaction of laser light with matter in the liquid phase has been comparatively less studied with respect to gas and solid phases. Nevertheless, some important features are well understood [8]. In the passage from gas to liquid phase, the energy separation between the energy levels reduces. This is sketched in figure 8, where the energy levels of gas and liquid argon are compared. The ionization potential for argon gas is $I_p = 15.76\,\text{eV}$,[6] and four excited states potentially involved in a multiphoton process lie at 11.83, 11.72, 11.62 and 11.55 eV, respectively. For two-photon absorption, $\Delta J = 0, 2$, and hence only transitions to levels with $J = 0$ and $J = 2$ are allowed by conservation rules.

The effects leading to the energy shift can be summarized in the following formula [13]:

$$I_p^{\text{liquid}} = I_p^{\text{gas}} + P_+ + V_0, \tag{2}$$

---

[6] NIST—National Institute of Standards and Technology, NIST Chemistry WebBook, NIST Standard Reference Database No. 69.
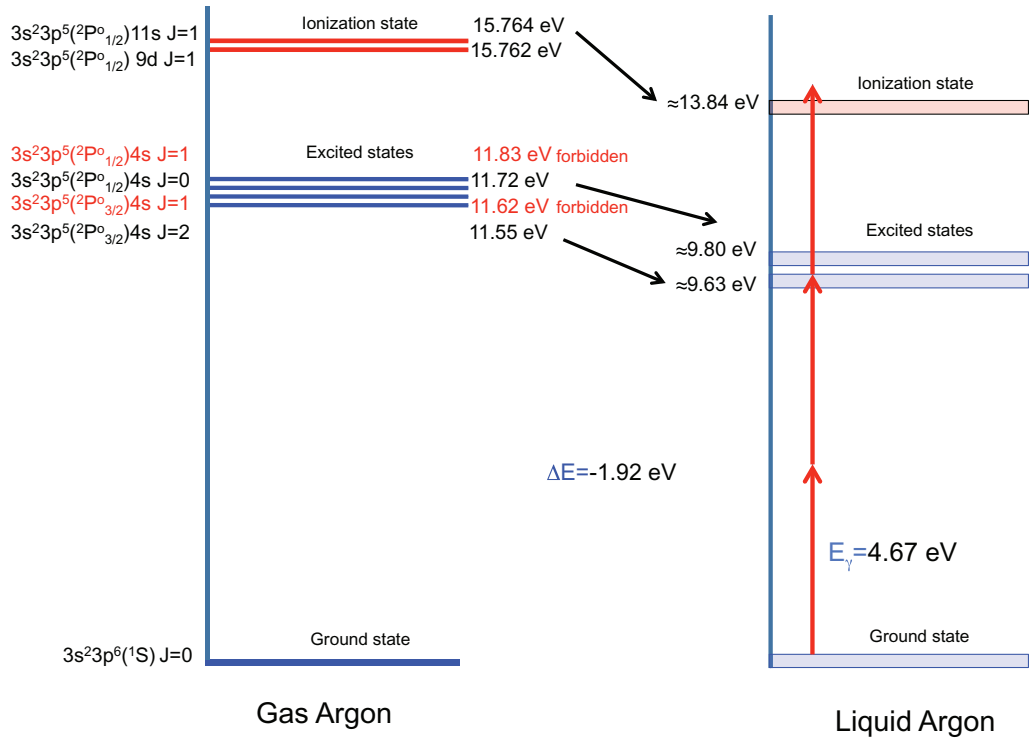
Figure 8. Schematics of the gas/LAr energetic levels. During the passage from gas to liquid phase, the absolute values of the energetic levels of the atom are reduced [8] and the lines broaden, becoming energy bands as in the condensed matter.

where I_p^{gas} (I_p^{liquid}) is the ionization potential in the gas (liquid) phase and V_0 is the energy of the quasi-free electron at the bottom of the conduction band of the liquid. The polarization energy P_+ of the positive ion is given by the Born equation [14]:

$$P_+ = -\frac{e^2}{2r_+}(1 - \epsilon^{-1}).\tag{3}$$

In the classical approximation, a liquid is treated as a uniform continuum with optical dielectric constant ϵ, while a positive ion is regarded as a sphere with radius r_+ and charge e. For argon the values experimentally measured are $\epsilon = 1.5$ at 550 nm and $\epsilon = 1.9$ at 128 nm, but extrapolation from a plot published in [16] leads to $\epsilon = 1.59$ at 266 nm. Since $V_0 = -0.17$ eV [15], $r_+ = 0.088$ nm, we have $P_+ = -1.75$ eV; thereby the ionization state in liquid turns out to be $I_p^{liquid} = I_p^{gas} - 1.92$ eV. Consequently, the ionization and the lowest excited state energies become, respectively,

$$I_p^{liquid} = 13.84 \text{ eV}, \quad P_e^{liquid} = 9.63 \text{ eV}.\tag{4}$$

In our experiment, we have used the fourth harmonic ($\lambda = 266$ nm, corresponding to a photon energy of 4.67 eV) of a Nd-YAG laser source, the main features of which are reported in table 1.

At this wavelength at least three photons are needed to produce ionization in LAr, although the intermediate real state can make the actual multiphoton transition a 2 + 1 transition. The

Table 1. Fourth-harmonic UV laser specifications (continuum, model Surelite I-10).

Wavelength (nm)	Max rep. rate (Hz)	Max energy (mJ)	Energy stability
266	10	82	5%
Pulse width (ns)	Rod diameter (mm)	Divergence (mrad)	FWHM (ns)
5–7	6	0.6	5.7

lowest allowed excited state is estimated to be at 9.63 eV, which is 0.3 eV higher than the energy of two photons at 266 nm. However, one has to consider that atomic energy levels broaden in the liquid phase [8] and that the energy shift of $\Delta E = -1.92\,\text{eV}$ could be underestimated due to approximations underlying our calculation, i.e. the true shift should be larger (2.2 eV) so as to move the two excited level bands below 9.5 eV, thereby matching the resonant two-photon absorption. It is worth mentioning that such a shift produces an energy gap free to VUV photon propagation, which is in total agreement with the well-known transparency of LAr to its own scintillation light at 128 nm (i.e. 9.7 eV), the latter being produced by the decay of excimers formed by particle energy loss.

4.2. Rate equations

In a multiphoton ionization process, the N-photon ionization rate W is given by $W = \sigma_N F^N$, where σ_N is the generalized N-photon ionization cross-section. The rate W is expressed in reciprocal seconds, σ_N is expressed in $\text{cm}^{2N}\,\text{s}^{N-1}$ and the laser flux F is in photon $\text{cm}^{-2}\,\text{s}^{-1}$.

For gases, the one-photon absorption cross-section σ_1 is typically of the order of $10^{-17}\,\text{cm}^2$ [19], whereas the two- and three-photon cross-sections are of the order of $\sigma_2 = W/F^2 \sim 10^{-50}\,\text{cm}^4\,\text{s}$ and $\sigma_3 = W/F^3 \sim 10^{-83}\,\text{cm}^6\,\text{s}^2$, respectively.

From the energy levels depicted in figure 8, we can write the following rate equation to retrieve the expected rate of excited electrons produced:

$$\frac{\mathrm{d}N_{\text{ex}}}{\mathrm{d}t} = (N_0 - N_{\text{ex}})F^2\sigma_{\text{ex}} - N_{\text{ex}}\sigma_i F - N_{\text{ex}}/\tau, \tag{5}$$

where N_0 is the initial density of atoms in the ground state, N_{ex} is the density of atoms in the excited state, σ_{ex} is the two-photon transition cross-section from the ground state to the intermediate excited state, σ_i is the single-photon transition cross-section from the excited state to the continuum and τ is the lifetime of the excited state. The rate of ionization is given by

$$\frac{\mathrm{d}N_i}{\mathrm{d}t} = N_{\text{ex}}\sigma_i F, \tag{6}$$

where N_i is the density of ionized atoms (or number of extracted electrons). Here we consider the ion/electron recombination (analyzed in section 3) to be negligible for UV laser-induced events at our operational drift field. Defining $h = \sigma_{\text{ex}}F^2 + \sigma_i F + (1/\tau)$, replacing equation (5) in equation (6) and time-integrating ($\Delta t = s$), one obtains

$$N_i = \frac{N_0\sigma_i\sigma_{\text{ex}}F^3}{h}\left(\frac{\mathrm{e}^{-hs} - 1}{h} + s\right), \tag{7}$$

where s is the FWHM of the laser pulse (in our case $s = (5.7 \pm 5\%) \times 10^{-9}\,\text{s}$).
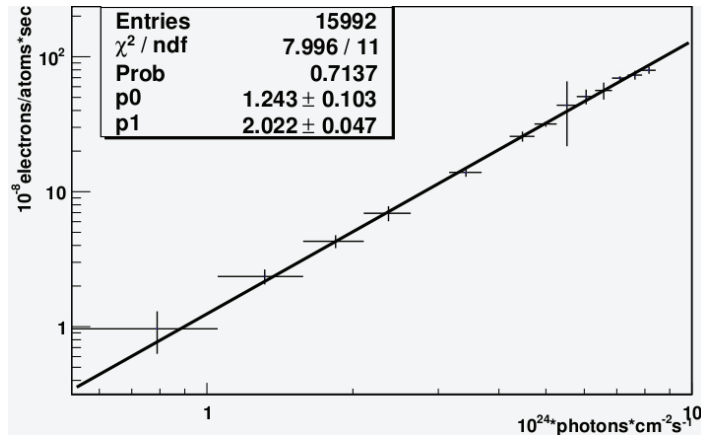
Figure 9. Profile histogram of the rate of electrons as a function of the photon flux of the laser beam.

Three different regions can be defined:

- low photon flux for $hs \ll 1$;
- high photon flux for $hs \gg 1$, $\sigma_{ex}F^2 \ll \sigma_i F$ and $1/\tau \ll \sigma_i F$;
- very high photon flux for $hs \gg 1$, $\sigma_{ex}F^2 \gg \sigma_i F$ and $1/\tau \ll \sigma_{ex}F^2$.

In the region of low photon flux, equation (7) can be written as

$$N_i = \tfrac{1}{2} N_0 \sigma_{ex} \sigma_i s^2 F^3, \tag{8}$$

showing a cubic dependence of the density of electrons in the ionized state with respect to the flux of photons. In the high photon flux regime, equation (7) becomes

$$N_i = N_0 \sigma_{ex} s F^2, \tag{9}$$

exhibiting quadratic dependence. Finally, for very high photon flux, equation (7) can be approximated as

$$N_i = N_0 \sigma_i s F, \tag{10}$$

with linear dependence due to saturation of the two-photon transition.

5. Results and data analysis

In order to estimate the cross-sections σ_{ex} and σ_i of the rate equations presented above, and the lifetime of the excited state of LAr, we measured the rate of electrons produced by the laser beam as a function of photon flux. For each laser track, we determined the total electron yield produced by the laser (for each wire) simultaneously, monitoring pulse by pulse the energy and FWHM of the beam. For the data set shown below, the beam energy was varied in the range 0.1–2.0 mJ.

Figure 9 reports the rate of electrons (measured in electron atom^{-1} s^{-1}) as a function of photon flux (measured in photon cm^{-2} s^{-1}) in a log–log plot. In the investigated intensity range the data are well described by a straight line, and the experimental points are very well fitted

IOP Institute of Physics **Φ** DEUTSCHE PHYSIKALISCHE GESELLSCHAFT

with a power law dependence on the photon flux F (see (8)–(10)). In particular, the best fit is obtained by using equation (9) in the following form:

$$\frac{N_i}{N_0 s} = \sigma_{ex} \cdot F^n, \tag{11}$$

with n and σ_{ex} as free parameters. The corresponding best fitted values are

$$n = 2.02 \pm 0.05, \tag{12}$$

$$\sigma_{ex} = (1.24 \pm 0.10_{stat} \pm 0.30_{syst}) \times 10^{-56}\,\text{cm}^4\,\text{s}. \tag{13}$$

The value of n is consistent with 2, indicating that at our laser intensities the limiting step of the three-photon ionization process is the two-photon absorption to the intermediate state.

The value of σ_{ex} presented here provides reliable and accurate measurements of the two-photon absorption cross-section of LAr. It is within the range of the two-photon absorption cross-section for liquids [17, 18]. The assumptions made ($hs \gg 1$, $(1/\tau) \ll \sigma_i F$ and $\sigma_i F \gg \sigma_{ex} F^2$) to approximate equation (7)–(9) to equation are justified by the experimental data. Moreover, the limits obtained for $\sigma_i > 5 \times 10^{-16}\,\text{cm}^2$ and $\tau > 10^{-9}\,\text{s}$ are consistent with the values $\sigma_i = 10^{-16}$–$10^{-17}\,\text{cm}^2$ and $\tau = 10^{-7}$–$10^{-8}\,\text{s}$ provided in [19]–[21].

Systematic uncertainties due to the absolute energy calibration of the TPC and to the measurement of the photon flux have been evaluated. We assume a 25% uncertainty on the absolute number of electrons collected, and a 10% uncertainty on the pulse-by-pulse measurement of the beam energy.

While our results for σ_i and τ are in reasonable agreement with those reported in [9], a disagreement of nearly three orders of magnitude is found for the value of σ_{ex}. The reason for such a large difference is not completely understood at this stage. However, one can make some considerations. In particular, no uncertainty on the estimation of σ_{ex} is given in [9]; thus the significance cannot be evaluated. As described before, in our experimental setup, particular care was taken in the photon flux measurement. The energy of the beam and the FWHM was performed pulse to pulse. The energy was measured by two different devices: a fast photodiode placed before the beam was actually steered in the TPC and an energy meter was placed at the end of the laser path. The FWHM was monitored by a fast analog-to-digital converter (ADC) board with 0.5 ns sampling. In this way, we kept the uncertainties low. Moreover, thanks to the spatial reconstruction capabilities of the TPC, we could select for the analysis laser pulses with uniform charge distribution along the track. This is very important for this measurement, since multiphoton absorption is not a linear process. In particular, we also noticed that prior to the installation of the optical feedthrough we observed a large non-uniform ionization in the tracks. This is probably due to a focusing/defocusing effect of the laser beam in the passage between the gas/liquid argon interface inside the detector. Data taken in these conditions provided on average less charge collected per track.

6. Conclusions and outlook

We reported on the measurement of UV laser-induced multiphoton ionization of LAr performed with a LAr TPC detector. For the first time, the value of the two-photon absorption cross-section $\sigma_{ex} = (1.24 \pm 0.10_{stat} \pm 0.30_{syst}) \times 10^{-56}\,\text{cm}^4\,\text{s}^{-1}$ has been determined with an accuracy appropriate for quantitative calibration of LAr TPC detectors. The systematic uncertainties on the value of σ_{ex} could be reduced even further by improving the accuracy of the TPC

calibration. Further measurements in the range of low photon flux ($hs \ll 1$) will be performed for a precise determination of the single-photon transition cross-section from the excited state to the continuum σ_i and the lifetime τ of the lower excited state of the LAr. The sensitivity to a lower flux of photons can be improved in several ways: first, with a different position (angle) of the TPC collection wire plane with respect to the laser tracks, in order to increase the portion of charge collected per wire; second, by improving the present charge preamplifiers (e.g. working in cold environments), providing a better signal-to-noise ratio; third, by using a different readout device with electron amplification, such as the large electron multiplier [22].

The results obtained and described in this paper make us confident about the practical use of UV laser beam techniques for the calibration of LAr TPC detectors, as required for the envisioned large-scale applications of the technique.

Acknowledgments

References

[1] Ankowski A *et al* 2006 Measurement of through-going particle momentum by means of multiple scattering with the ICARUS T600 TPC *Eur. Phys. J.* C **48** 667

[2] Rossi B *et al* 2009 A prototype liquid argon time projection chamber for the study of UV laser multi-photonic ionization *J. Inst.* JINST **4** P07011

[3] Ereditato A and Rubbia A 2005 Ideas for future liquid argon detectors *Nucl. Phys. Proc. Suppl.* **139** 301

[4] Ereditato A and Rubbia A 2006 The liquid argon TPC: a powerful detector for future neutrino experiments and proton decay searches *Nucl. Phys. Proc. Suppl.* **154** 163

[5] Ereditato A and Rubbia A 2006 Conceptual design of a scalable multi-kton superconducting magnetized liquid argon TPC *Nucl. Phys. Proc. Suppl.* **155** 233

[6] Baibussinov B *et al* 2007 A new, very massive modular liquid argon imaging chamber to detect low energy off-axis neutrinos from the CNGS beam (project MODULAr) arXiv:0704.1422

[7] Autiero D *et al* 2007 Large underground, liquid based detectors for astro-particle physics in Europe: scientific case and prospects *J. Cosmol. Astropart. Phys.* JCAP11(2007)011

[8] Schmidt W F 1984 Electronic conduction processes in dielectric liquids *IEEE Trans. Electr. Insul.* **EI-19** 389

[9] Sun J, Cao D and Dimmock J 1996 Investigating laser-induced ionization of purified liquid argon in a time projection chamber *Nucl. Instrum. Methods Phys. Res.* A **370** 372

[10] Ereditato A *et al* 2008 Study of ionization signals in a TPC filled with a mixture of liquid argon and nitrogen *J. Inst.* JINST **3** P10002

[11] Messer Schweiz A G http://www.messer.ch

[12] Chin S L and Lambropoulos P 1984 *Multiphoton Ionization of Atoms* (Toronto: Academic Press)

[13] Raz B and Jortner J 1969 Energy of the quasi-free electron state in liquid and solid rare gases *Chem. Phys. Lett.* **4** 155

[14] Born M 1920 Volumen und Hydratationswaerme der Ionen *Z. Phys.* **1** 45

[15] Reininger R, Asaf U, Steinberger I T and Basak S 1983 Relationship between the energy V0 of the quasi-free-electron and its mobility in fluid argon, krypton and xenon *Phys. Rev.* B **28** 4426

[16] Antonello M *et al* 2004 Detection of Cherenkov light emission in liquid argon *Nucl. Instrum. Methods Phys. Res.* A **516** 348

[17] Tam A C and Patel C K N 1979 Two-photons absorption spectra and cross-section measurements in liquids *Nature* **280** 304–6

[18] Elles C G *et al* 2009 Electronic structure of liquid water from polarization-dependent two-photon absorption spectroscopy *J. Chem. Phys.* **130** 084501

[19] Hilke H J 1986 Detector calibration with lasers—a review *Nucl. Instrum. Methods Phys. Res.* **252** 169

[20] Bourotte J and Sadoulet B 1980 Ionization of multiwire proportional chamber gas by double photon absorption *Nucl. Instrum. Methods* **173** 463

[21] Hurst G S *et al* 1979 Resonance ionization spectroscopy and one-atom detection *Rev. Mod. Phys.* **51** 767

[22] Badertscher A *et al* 2008 Construction and operation of a double phase LAr large electron multiplier time projection chamber arXiv:0811.3384